Title

Differential effects of serine side chain interactions in amyloid formation by islet amyloid polypeptide

Permalink

https://escholarship.org/uc/item/6bb8590d

Authors

Akter, Rehana
Zou, Junjie
Raleigh, Daniel P

Peer reviewed

ARTICLE

Differential effects of serine side chain interactions in amyloid formation by islet amyloid polypeptide

Rehana Akter[1] | Junjie Zou[1,2] | Daniel P. Raleigh[1,2]

[1]Department of Chemistry, Stony Brook University, Stony Brook, New York

[2]Laufer Center for Physical and Quantitative Biology, Stony Brook University, Stony Brook, New York

Correspondence
Daniel P. Raleigh, Department of Chemistry, Stony Brook University, Stony Brook, New York.
Email: daniel.raleigh@stonybrook.edu

Funding information
National Institutes of Health, Grant/Award Number: GM078114

Abstract

Islet amyloid polypeptide (IAPP), a 37 residue polypeptide, is the main protein component of islet amyloid deposits produced in the pancreas in Type 2 diabetes. Human IAPP contains five serine residues at positions 19, 20, 28, 29, and 34. Models of the IAPP amyloid fibril indicate a structure composed of two closely aligned columns of IAPP monomers with each monomer contributing to two intermolecular β-strands. Ser 19 and Ser 20 are in the partially ordered β-turn region, which links the two strands, whereas Ser 28, Ser 29, and Ser 34 are in the core region of the amyloid fibril. Ser 29 is involved in contacts between the two columns of monomers and is the part of the steric zipper interface. We undertook a study of individual serine substitutions with the hydrophobic isostere 2-aminobutyric acid (2-Abu) to examine the site-specific role of serine side chains in IAPP amyloid formation. All five variants formed amyloid. The Ser 19 to 2-Abu mutant accelerates amyloid formation by a factor of 3 to 4, while the Ser 29 to 2-Abu mutation modestly slows the rate of amyloid formation. 2-Abu replacements at the other sites had even smaller effects. The data demonstrate that the cross-column interactions made by residue 29 are not essential for amyloid formation and also show that cross-strand networks of hydrogen-bonded Ser side chains, so called Ser-ladders, are not required for IAPP amyloid formation. The effect of the Ser 19 to 2-Abu mutant suggests that residues in this region are important for amyloid formation by IAPP.

KEYWORDS

amylin, amyloid, IAPP, Ser-ladders, Type 2 diabetes

1 | INTRODUCTION

The aggregation of soluble polypeptides and proteins to self-assemble into ordered, stable amyloid fibrils is a key feature of many neurodegenerative diseases including Alzheimer's disease and Parkinson's disease, Prion-based diseases, and Type 2 diabetes.[1–6] Postmortem analysis of Type 2 diabetes patients indicates that up to 90% exhibited islet amyloid deposits in the pancreas.[7,8] The neuropancreatic

hormone islet amyloid polypeptide (IAPP), also known as amylin, is the major protein component of islet amyloid deposits.[7,9] IAPP plays an important role as an adjunct to insulin in glycemic control and is coexpressed, costored, and cosecreted from the β-cells with insulin in response to glucose stimuli.[6,10] The polypeptide slows gastric emptying and helps control satiety[11]; however, IAPP amyloid formation contributes to β-cell death, the loss of β-mass in Type 2 diabetes, and the failure of transplanted islet grafts.[12–16]

IAPP is a 37-residue polypeptide with a conserved disulfide bridge between residues 2 and 7 and an amidated C-terminus. The polypeptide is relatively hydrophobic; however, IAPP contains a significant number of noncharged polar residues, notably human IAPP contains five serine residues at positions 19, 20, 28, 29, and 34 (Figure 1). IAPP is found in all higher-order species and the sequence is highly conserved among species; the most divergent region is within residues 20 and 29 (Table S1). The naturally occurring IAPP S20G missense mutation has been detected at low levels in Asian populations and has been proposed to be related to a higher risk of diabetes.[17–19] in vitro studies report that the S20G mutant accelerates IAPP amyloid formation and cytotoxicity to β-cells.[20–22] The role of the other Ser residues has not been studied, and the only reported studies of Ser 20 substitutions have involved Gly or Lys replacements.[21]
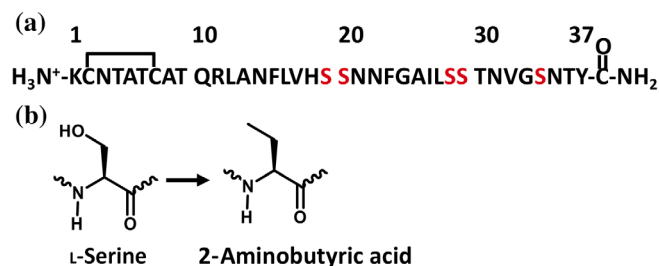
Rat IAPP is nonamyloidogenic, and rat IAPP has prolines at positions 28 and 29 instead of Ser. Both Ser 19 and 34 are highly conserved in known IAPP sequences (Table S1).

The molecular mechanism of IAPP amyloid formation is not known, conformations of prefibrillar oligomeric species are not defined, nor are the key residues which are involved in amyloid formation known, and the interactions that stabilize the fibril are not fully understood. In this study, we replaced each serine with the unnatural amino acid 2-aminobutyric acid (2-Abu) and examined the effects on amyloid formation. 2-Abu is a nonpolar, isosteric analog of serine (Figure 1). The work provides new insights into the role of specific side chain interactions in IAPP amyloid formation.

2 | RESULTS AND DISCUSSION

We systematically scanned all five Ser residues with 2-Abu to examine the role played by the polar groups in Ser side chains in the amyloid formation by IAPP. A Ser to 2-Abu substitution replaces the hydroxyl group attached to the β-carbon with a methyl group and thus closely retains the shape and the volume of Ser. 2-Abu is more hydrophobic than Ser and has been reported to have a higher helical propensity (Table 1). We prepared five single-substituted Ser to 2-Abu variants using solidphase peptide synthesis.

The five Ser residues are in unique environments in the IAPP amyloid fibril (Figure 2). There are two similar high-resolution models of the IAPP amyloid fibril, one developed based on solid-state nuclear magnetic resonance (NMR) studies and the other from X-ray crystallography studies of small fragments of IAPP.[26,27] Both models indicate that the IAPP fibril is made up of two symmetrical columns of U-shaped IAPP monomers, with each monomer containing two β-strands separated by a partially ordered loop (Figure 2). In each layer of the IAPP fibril residues in the C-terminal β-sheet of IAPP monomers from different columns are interdigitated to form the core of the fibril. Ser 19 and Ser 20 are in the loop region and Ser 28, Ser 29, and Ser 34 are part of the C-terminal β-strand

FIGURE 1 (a) The primary sequence of human IAPP. IAPP contains five serine residues in the sequence, which are colored red. IAPP contains an intramolecular disulfide bond between residues Cys2 and Cys7 and has an amidated C-terminus. (b) The structure of L-serine and 2-aminobutyric acid (2-Abu)

TABLE 1 A comparison of the properties of serine and 2-aminobutyric acid

Amino acid	Hydrophobicity[a]	Normalized VDW volume relative to alanine[23]	α-Helix propensity
Serine	−0.04	1.60	Approximately half the value for alanine[24]
2-Aminobutyric acid	0.82	2.00	Equivalent to alanine[25]

[a]Based on log p (amino acid)–log p (glycine).[23]

(a)

(b)
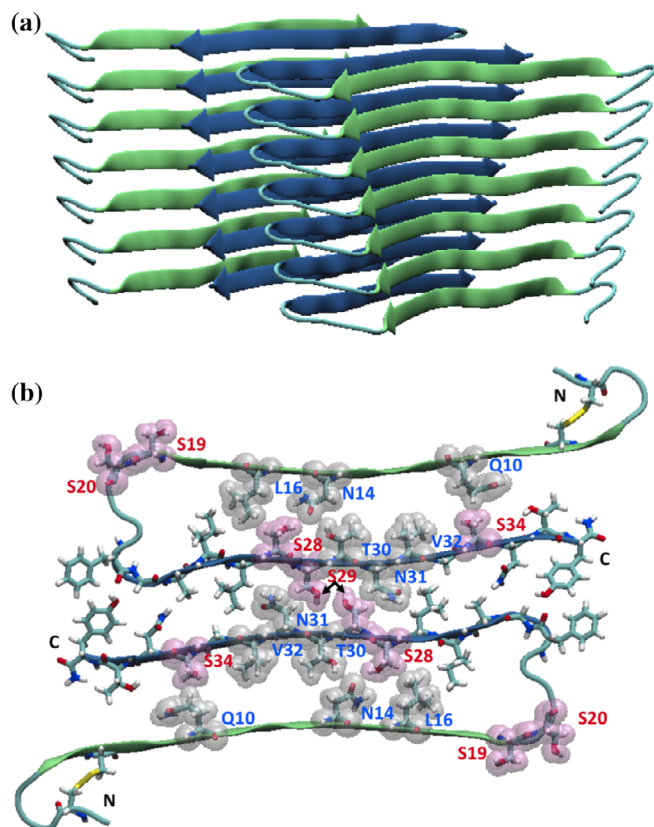
FIGURE 2 (a) A side view of the structure of the model of the IAPP fribl shown in ribbon view presentation. The β-strands in the N-terminal region are colored green and those in the C-terminal are blue. (b) A top down view of the IAPP fibril model developed based on X-ray crystal structure of small fragments of IAPP.[26] The five serine residues (pink space filling and stick format with red lettering) together with key interacting residues (gray space filling and stick format with blue lettering) and other residues in the steric zipper interface of the IAPP fibril (stick format). The N- and C-termini are labeled. IAPP, islet amyloid polypeptide

TABLE 2 Fractional solvent accessibility (SASA) of the serine side chains in the X-ray and solid-state NMR models of the IAPP amyloid fibril relative to a reference tripeptide in an extended conformation

Panel (a) Residue		Fractional SASA
Ser 19		0.72
Ser 20		0.73
Ser 28		0.04
Ser 29		0
Ser 34		0.19
Panel (b) Residue	Fractional SASA, chain A	Fractional SASA, chain B
Ser 19	0.80	0.05
Ser 20	0.65	0.70
Ser 28	0.36	0.01
Ser 29	0.12	0.26
Ser 34	0.25	0.54

Notes: (a) Fibril model developed from X-ray crystallography of peptide fragments and (b) fibril model developed from solid state NMR. The two polypeptide chains in one layer of the solid-state NMR model are not symmetrical and thus the Ser residues in the chains do not have the same SASA values.

in the core of the fibril backbone. Ser 28 and Ser 34 face into the intramolecular core of one column of monomers of the fibril, while the Ser 29 side chain projects into the interface between the two columns.

The main chain hydrogen bonds in both models are formed between different IAPP molecules located in the same column, and there are no intramolecular backbone hydrogen bonds. The interface between the two columns is tightly packed and, in the X-ray based model, includes residues 23 to 37 (Figure 2). The Ser 28 side chain interacts with the side chain of Asn 14, Leu 16, and Thr 30 in the same polypeptide and with Ser 28 residues located in the same column one chain above and one chain below. The Ser 29 side chain, in contrast, interacts with Ser 29 and Asn 31 in the other polypeptide chain within the same layer. It also interacts with Ser 29 residues located in the same

column one chain above and one chain below. The side chain of Ser 34 interacts with Gln 10 and Val 32 of the same polypeptide chain and with Ser 34 residues in the chains immediately above and below within the same column. The interactions between Ser residues located above and below each other in the same column resemble those made by Asn and Gln residues. In the sense that all involve potential interstrand hydrogen bonded networks, so-called Asn and Gln "ladders", have been proposed to stabilize amyloid fibrils.[28–31]

All of the Ser residues adopt conformations which fall in the allowed region of the Ramachandran plot. The fractional solvent accessibility of the Ser side chains, defined relative to a reference tripeptide, range from 72 and 73% for Ser 19 and Ser 20 to 4 and 0% for Ser 28 and Ser 29, and 19% for Ser 34 based on the X-ray model. Similar trends are observed in the solid-state NMR model; Ser 19 and Ser 20 are the most exposed and Ser 28 and Ser 29 are the least exposed (Table 2).

We first used computational energy decomposition to test if any of the Ser side chains make unfavorable steric interactions in the high-resolution models of the IAPP amyloid fibril. We then repeated the calculations for the 2-Abu replacements. We changed each Ser to 2-Abu in both the X-ray and solid-state NMR models and conducted energy minimization with restraint of the backbone to allow

relaxation of the structures. Energy decomposition was conducted for three central layers of each structure. In all cases, the calculated van der Waals (VDW) interactions were negative (favorable) for Ser in both models and were negative or zero for all 2-Abu residues in both models (Table 3). Furthermore, the values calculated for Ser and 2-Abu are correlated with each other. This analysis argues that any effects caused by a 2-Abu replacement are not due to the relief of or the introduction of steric clashes involving the side chain in the amyloid fibril.

We also examined the consequences of the 2-Abu substitutions in the context of monomeric IAPP. Monomeric human IAPP does not fold to a defined globular tertiary structure; however structures have been reported for human IAPP at low pH and for the polypeptide bound to micelles. We repeated the analysis using these

structures (PDB codes: 2L86, 2KB8, 5M6Q). In all cases, the VDW interactions were negative (favorable) for all Ser and 2-Abu residues. This indicates, within the limitations of these structural models, that there are no steric clashes in the monomer state. Thus, the differential effects of the 2-Abu substitution cannot be rationalized based on steric effects in the monomers or fibrils (Table S2).

We monitored the rate of amyloid formation using fluorescence-detected thioflavin T binding assays. Thioflavin T is a small fluorescence dye, commonly used to monitor amyloid formation.[32] It has a low quantum yield in solution, which increases when the dye binds to amyloid fibrils. However, thioflavin T assays can give false negatives; hence, we also confirmed amyloid formation using transmission electron microscopy (TEM).

We first examined the effects of Ser to 2-Abu substitutions in the loop region. Thioflavin T assays and TEM measurements show that both S19 2-Abu IAPP and S20 2-Abu IAPP form amyloid (Figure 3). We compared the T_{50} of S19 2-Abu IAPP and S20 2-Abu IAPP with the T_{50} of wild-type IAPP (Table 4), where T_{50} is the time at which the thioflavin T fluorescence intensity reaches half of its final value. T_{50} is a standard parameter commonly used to compare the rate of amyloid formation. The T_{50} values of wild-type peptide, S19 2-Abu IAPP, and S20 2-Abu IAPP are 17.0 ± 4.0, 4.9 ± 0.7, and 14.7 ± 1.4 hr,

TABLE 3 van der Waals (VDW) contributions of serine and 2-aminobutyric acid side chains in the X-ray and solid-state NMR based models of the IAPP amyloid fibril

Panel (a) Residue	VDW energy (kcal/mol)	
Abu19	−2.3	
Abu20	−1.4	
Abu28	−4.7	
Abu29	−6.4	
Abu34	0.1	
Ser19	−2.5	
Ser20	−1.6	
Ser28	−4.5	
Ser29	−5.7	
Ser34	−0.4	
Panel (b) Residue	VDW energy (kcal/mol), chain A	VDW energy (kcal/mol), chain B
Abu19	−2.1	−5.7
Abu20	−3.3	−3.6
Abu28	−4.9	−4.8
Abu29	−6.2	−5.5
Abu34	−4.6	−4.2
Ser19	−2.2	−7.8
Ser20	−3.2	−3.6
Ser28	−4.7	−4.1
Ser29	−5.9	−5.2
Ser34	−5.3	−4.1

Notes: (a) Fibril model developed from X-ray crystallography and (b) fibril model developed from solid state NMR. Since the IAPP monomers are not symmetric in the two columns in NMR model, the VDW interaction energy is calculated for both monomers.

FIGURE 3 (a) Thioflavin T fluorescence-monitored kinetic experiments comparing the rate of amyloid formation. Representative curves are shown: wild-type APP (black), S19 2-Abu IAPP (red), and S20 2-Abu IAPP (blue). All experiments were conducted using 16 μM peptide in 20 mM Tris–HCl buffer at pH 7.4 and at 25°C. (b) TEM images of IAPP, S19 2-Abu, and S20 2-Abu mutants. TEM images collected at the end of the kinetics experiments. Scale bar represents 100 nm. IAPP, islet amyloid polypeptide; TEM, transmission electron microscopy

TABLE 4 Summary of values of T_{50} for IAPP and Ser to 2-Abu variants

Peptide	T_{50} (hr)
Wild-type IAPP	17.0 ± 4.0
S19 2-Abu IAPP	4.9 ± 0.7
S20 2-Abu IAPP	14.7 ± 1.4
S28 2-Abu IAPP	15.3 ± 2.6
S29 2-Abu IAPP	32.2 ± 5.4
S34 2-Abu IAPP	20.4 ± 1.7

Note: The quoted uncertainties are the estimated *SDs*.

respectively (Table 4). The analysis shows that the time course of amyloid formation by S20 2-Abu IAPP is similar to that of the wild-type peptide, but that the rate of amyloid formation by S19 2-Abu IAPP is faster (Figure 3) with the Ser 19 to 2-Abu replacement accelerating amyloid formation about three- to four-fold compared with wild-type IAPP. This argues that the terminal methyl group of 2-Abu at position 19 makes more favorable interactions during amyloid formation than those of the Ser 19 hydroxyl group (or less unfavorable interactions). These could include more favorable packing interactions formed by the methyl group, a smaller desolvation penalty for the 2-Abu side chain, or the avoidance of unproductive hydrogen bonding interactions involving the Ser-19 hydroxyl.

We next examined the effects of serine to 2-Abu substitution in the β-strand region. The thioflavin T data and TEM analysis show that S28 2-Abu IAPP, S29 2-Abu IAPP, and S34 2-Abu IAPP all form amyloid (Figure 4). The kinetics data reveal that the effect on the rate of amyloid formation is modest for all three variants. S29 2-Abu IAPP had the most substantial effect compared with the other two variants, but the measured T_{50} was only 90% larger than that of wild type. The T_{50} values for S28 2-Abu IAPP, S29 2-Abu IAPP, and S34 2-Abu IAPP are 15.3 ± 2.6, 32.2 ± 5.4, and 20.4 ± 1.7 hr, respectively (Table 4).

No apparent difference in fibril morphology among the variants was detectable by TEM (Figure 3, Figure 4). However, amyloid formation can lead to different polymorphs. Formation of IAPP polymorphs is well documented, and not all are detectable by TEM.[33–36] Thus, we cannot rule out that the variant peptides studied here may produce different polymorphic forms of IAPP amyloid, and it is worth reiterating that one of the Ser residues is located in the zipper like interface between the two columns. However, our calculations show that both the Ser and 2-Abu side chains can be accommodated into the two different high-resolution models of the IAPP amyloid fibril without introducing unfavorable steric
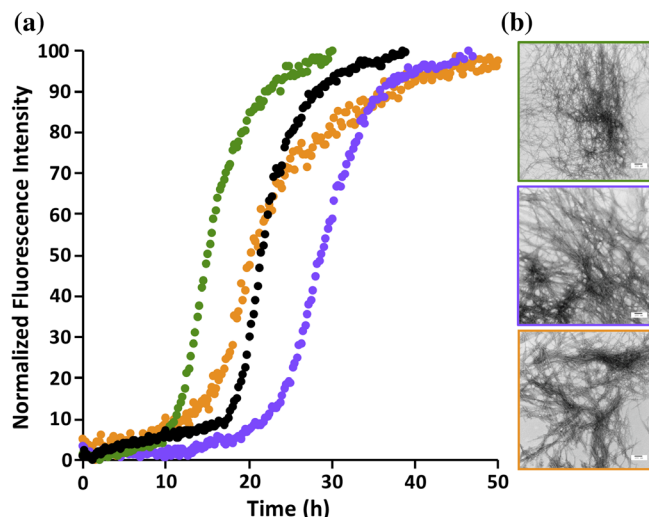
FIGURE 4 (a) Thioflavin T fluorescence-monitored kinetic experiments comparing the rate of amyloid formation. Representative curves are shown: wild type IAPP (black), S28 2-Abu IAPP (green), S29 2-Abu IAPP (purple), and S34 2-Abu IAPP (orange). All experiments were conducted using 16 μM peptide in 20 mM Tris–HCl buffer at pH 7.4 and at 25°C. (b) TEM images of S28 2-Abu, S29 2-Abu, and S34 2-Abu mutants. TEM images collected at the end of the kinetics experiments. Scale bar represents 100 nm. IAPP, islet amyloid polypeptide; TEM, transmission electron microscopy

clashes, and the experimental data shows that all variants readily form amyloid.

3 | CONCLUSIONS

Replacement of the Ser hydroxyl group with a methyl group removes the possibility of hydrogen bond interactions and also eliminates the desolvation penalty of burying a polar hydroxyl group in a hydrophobic environment, while preserving side chain shape and volume. It thus represents a considerably more conservative substitution than the ones available with the 20 genetically coded amino acids. In the present case, this has allowed us to explore the role made by hydroxyl group hydrogen bonds and potential desolvation effects while minimizing other perturbations. The data presented here indicate that, with the exception of position 19, hydrogen bond and other interactions made by the serine hydroxyl groups have modest effects on amyloid formation relative to those made by a hydrophobic isostere. This shows that interstrand hydrogen bond interactions made by a "ladder" of Ser side chains are not critical for IAPP amyloid formation. The data also show that the interactions made by the hydroxyl group of the Ser at position 19 are less favorable for amyloid formation than those made by the methyl group in the hydrophobic isostere, as amyloid formation is faster when the hydroxyl is replaced by a

methyl group. The molecular origin of these effects cannot be deduced from the present data, but possibilities include that the terminal methyl group of the 2-Abu side chain at residue 19 makes more favorable interactions during amyloid formation relative to the Ser 19 hydroxyl group, or diminishes unfavorable interactions formed by the wild-type side chain, or reduces interactions that promote the formation of off-pathway species, or alters backbone structural propensities in a way that promotes amyloid formation. These effects could include a smaller desolvation penalty for the 2-Abu side chain relative to a Ser side chain, or the formation of more favorable packing by the methyl group, or the avoidance of unproductive hydrogen bonding interactions involving the Ser-19 hydroxyl.

The fact that the most potent effect was observed for the Ser 19 to 2-Abu replacement reinforces the sensitivity of the turn region in amyloid formation. Ser 19 and Ser 20 are both in the turn region in the fibril models, and the data suggest that the side chains of these two residues have different roles in amyloid formation given that 2-Abu substitutions at these sites have different effects. There are no structures of pre-amyloid oligomers formed by full-length IAPP, so it is not possible to directly ascribe a role to the Ser 19 and Ser 20 side chains. Techniques such as two-dimensional IR spectroscopy combined with specific isotopic labeling can prove residue-specific backbone conformational information in a time-resolved fashion and might provide more insight into the role of Ser-19; however, the experiments require considerably higher peptide concentrations than used here and it is currently difficult to structurally probe specific Ser side chains.[37–39]

The modest reduction in the rate of amyloid formation by S29 2-Abu IAPP compared with wild type is interesting as Ser-29 is part of the interface between the two columns of IAPP molecules in both high-resolution models of IAPP amyloid. This shows that while interactions in the steric zipper interface involving the hydroxyl group at position 29 may stabilize the core of the fibril, they are not critical for amyloid formation. The other two Ser residues in the C-terminal β-strand region, Ser 28, and Ser 29, project into the interior of a column, and the lack of an effect upon their replacement by 2-Abu indicates that their hydroxyl groups do not make net key contributions to IAPP amyloid formation relative to a methyl substitution.

4 | MATERIALS AND METHODS

4.1 | Peptide synthesis and purification

Wild-type APP, S19 2-Abu IAPP, S20 2-Abu IAPP, S28 2-Abu IAPP, S29 2-Abu IAPP, and S34 2-Abu were synthesized using standard Fmoc (9-fluorenylmethoxycarbonyl) solid-phase methods with a CEM Liberty automated microwave peptide synthesizer. Polyamide linker poly-ethylene glycol polystyrene resin was used to obtain the amidated C-terminus. O-(benzotriazol-1-yl)-N,N,N′,N′- tetramethyluronium hexafluorophosphate and diisopropyl ethylamine were used as coupling agents. Fmoc-protected pseudoproline dipeptide derivatives were used at the positions 8–9, 19–20, and 27–28 to facilitate the synthesis except for S28 2-Abu where the pseudoproline was inserted at position 29–30 instead of at residue 27–28.[40] The first residue attached to the resin, pseudoproline-dipeptide derivatives, residues after pseudoproline dipeptides and all β-branched residues were double coupled. The peptides were cleaved and deprotected from the resin by treatment with trifluoroacetic acid (TFA) with 3% (v/v) anisole, 3% (v/v) thioanisole, and 3% (v/v) 1,2-ethanedithiol included as scavengers at room temperature for 3 hr, followed by cold diethylether precipitation. Solvents used were of American Chemical Society grade. Fmoc-protected pseudoproline (oxazolidine) dipeptide derivatives were purchased from Novabiochem. All other reagents were purchased from Advanced Chemtech, PE Biosystems, Sigma, and Fisher Scientific.

Crude peptides were partially dissolved in 20% acetic acid (v/v) to increase their solubility and were freeze-dried. The dry polypeptides were dissolved in 100% dimethyl sulfoxide and allowed to stand at room temperature for a minimum of 72 hr to promote the formation of the Cys-2-Cys-7 disulfide bond. The peptides were purified using reversed-phase HPLC with a Vydac C18 preparative column (10 mm X 250 mm). An A-B gradient system was used where buffer A consisted of 100% H_2O and 0.045% HCl (v/v) and buffer B consisted of 80% acetonitrile, 20% H_2O, and 0.045% (v/v) HCl. The gradient was 20–60% buffer B in 40 min or 20–70% buffer B in 50 min. The pure peptides usually eluted around 24 to 32 min. HCl was utilized as the ion-pairing agent instead of TFA since TFA can influence the rate of aggregation. After the initial purification, the peptide was redissolved in hexafluoro isopropanol (HFIP) and was subjected to a second round of HPLC purification. This procedure was used to remove residual scavengers. The purity of peptide was checked by HPLC using a Vydac C18 reversed-phase analytical column (4.6 mm × 250 mm). The identities of the purified peptides were confirmed by mass spectrometry using a Bruker MALDI-TOF MS (matrix-assisted laser desorption ionization time-of-flight mass spectrometry) instrument. The expected and observed molecular masses for oxidized wild-type IAPP, expected 3903.3, observed 3902.5; expected molecular masses for Ser to 2-Abu variants, 3901.3; S19 2-Abu IAPP observed 3902.7; S20 2-Abu IAPP, observed

3902.8; S28 2-Abu IAPP, observed 3901.6; S29 2-Abu IAPP, observed 3901.6; and S34 2-Abu IAPP, observed 3901.3.

4.2 | Sample preparation for thioflavin T binding kinetic assays

A 1.6 mM stock solution was prepared by dissolving dry peptide (stored at −20°C inside a desiccator) in 100% HFIP. The solution was filtered through a 0.22 μm Millex syringe-driven filter. Measured amounts of stock solution were aliquoted and lyophilized to remove the HFIP for concentration measurements. The concentration was determined using a Beckman Coulter UV/Vis spectrophotometer by measuring the absorbance at 280 nm.

Thioflavin T-binding fluorescence experiments were performed using a Beckman-Coulter DTX 880 multimode detector plate reader. Thioflavin T fluorescence was measured at 430 nm excitation wavelength and 485 nm emission wavelength. Corning 96-well nonbinding surface black plates with lids was used for the assay. Fluorescence intensity was detected from the bottom of the plate. The experiments were performed at 16 μM peptide concentration. Measured amounts of filter aliquots were lyophilized to remove HFIP. Lyophilized dry peptides were dissolved in 20 mM Tris–HCl buffer (pH 7.4) containing 32 μM thioflavin T solution. The final experimental conditions were as follows: 16 μM peptide, 32 μM thioflavin T, no HFIP, and pH 7.4 without stirring.

4.3 | Transmission electron microscopy

TEM images were obtained using an FEI EM microscope at the Life Science Microscopy Center at Stony Brook University. 15 μl peptide samples were taken out at the end of the kinetic experiments and was blotted onto a carbon-coated Formvar 300 mesh copper grid for 1 min and then negatively stained with saturated uranyl acetate for 1 min. Images were taken at 80 kV. Images were collected using a ×68,000 magnification and 100 nm under focus.

4.4 | Energy minimization and energy decomposition

Two IAPP fibril models, an X-ray model and a solid-state NMR model, were used for energy decomposition. The X-ray model is the minimized IAPP fibril model developed based on the structure of steric zipper fragments from X-ray crystallography. The methods for minimization of the X-ray model are described in detail by Marek et al.[41] tleap from the Amber18 software package was used for constructing

the Ser to 2-Abu mutant.[42] ff14sbonlysc and mbondi3 GBradii were used.[43] Parameters for the 2-Abu amino acids were adopted from Khoury et al.[44] The implicit solvent model GBneck2 were used for energy minimization.[43] The concentration of the salt was set to be 0. The backbone atoms (N, CA, and C) of the fibril were restraint using harmonic restraints with a strength of 999 kcal/mol. pmemd was used for energy minimization with a maximum cycle of 10,000. Sander was used to decompose the energy of the minimized fibril structures.

4.5 | Solvent accessible surface area calculations

The solvent accessible surface area (SASA) was calculated using a probe radius of 1.4 Å using visual molecular dynamics. A tripeptide sequence was built as a reference state for each Ser where the appropriate Ser was in the middle with the preceding and succeeding residues for each Ser in the IAPP sequence. The dihedral angle (φ, ψ) angles for all three residues in the reference peptide were set to (180°, 180°). The fractional SASA is the ratio of the SASA in the fibril to the SASA in the reference state peptide.

CONFLICT OF INTEREST
The authors declared no potential conflict of interest.

ORCID
Daniel P. Raleigh https://orcid.org/0000-0003-3248-7493

REFERENCES
1. Sipe JD. Amyloidosis. Crit Rev Cl Lab Sci. 1994;31:325–354.
2. Chiti F, Dobson CM. Protein misfolding, functional amyloid, and human disease. Annu Rev Biochem. 2006;75:333–366.
3. Soto C. Unfolding the role of protein misfolding in neurodegenerative diseases. Nat Rev Neurosci. 2003;4:49–60.
4. Cao P, Marek P, Noor H, et al. Islet amyloid: From fundamental biophysics to mechanisms of cytotoxicity. FEBS Lett. 2013; 587:1106–1118.
5. Selkoe DJ. Cell biology of protein misfolding: The examples of Alzheimer's and Parkinson's diseases. Nat Cell Biol. 2004;6: 1054–1061.
6. Westermark P, Andersson A, Westermark GT. Islet amyloid polypeptide, islet amyloid, and diabetes mellitus. Physiol Rev. 2011;91:795–826.

7. Cooper GJS, Willis AC, Clark A, Turner RC, Sim RB, Reid KBM. Purification and characterization of a peptide from amyloid-rich pancreases of type-2 diabetic-patients. Proc Natl Acad Sci U S A. 1987;84:8628–8632.

8. Westermark P, Grimelius L. Pancreatic-islet cells in insular amyloidosis in human diabetic and non-diabetic adults. Acta Path Micro Im A A. 1973;81:291–300.

9. Westermark P, Wernstedt C, Wilander E, Hayden DW, Obrien TD, Johnson KH. Amyloid fibrils in human insulinoma and islets of Langerhans of the diabetic cat are derived from a neuropeptide-like protein also present in normal islet cells. Proc Natl Acad Sci U S A. 1987;84:3881–3885.

10. Akter R, Cao P, Noor H, et al. Islet amyloid polypeptide: Structure, function, and pathophysiology. J Diabetes Res. 2016;2016:2798269.

11. Hay DL, Chen S, Lutz TA, Parkes DG, Roth JD. Amylin: Pharmacology, physiology, and clinical potential. Pharmacol Rev. 2015;67:564–600.

12. Kahn SE, Zraika S, Utzschneider KM, Hull RL. The beta cell lesion in type 2 diabetes: There has to be a primary functional abnormality. Diabetologia. 2009;52:1003–1012.

13. Raleigh D, Zhang XX, Hastoy B, Clark A. The beta-cell assassin: IAPP cytotoxicity. J Mol Endocrinol. 2017;59:R121–R140.

14. Potter KJ, Abedini A, Marek P, et al. Islet amyloid deposition limits the viability of human islet grafts but not porcine islet grafts. Proc Natl Acad Sci U S A. 2010;107:4305–4310.

15. Abedini A, Plesner A, Cao P, et al. Time-resolved studies define the nature of toxic IAPP intermediates, providing insight for anti-amyloidosis therapeutics. Elife. 2016;5:e12977.

16. Jurgens CA, Toukatly MN, Fligner CL, et al. Beta-cell loss and beta-cell apoptosis in human type 2 diabetes are related to islet amyloid deposition. Am J Pathol. 2011;178:2632–2640.

17. Sakagashira S, Sanke T, Hanabusa T, et al. Missense mutation of amylin gene (S20G) in Japanese NIDDM patients. Diabetes. 1996;45:1279–1281.

18. Lee SC, Hashim Y, Li JKY, et al. The islet amyloid polypeptide (amylin) gene S20G mutation in Chinese subjects: Evidence for associations with type 2 diabetes and cholesterol levels. Clin Endocrinol (Oxf). 2001;54:541–546.

19. Seino S, Genet SGCA. S20G mutation of the amylin gene is associated with type II diabetes in Japanese. Diabetologia. 2001;44:906–909.

20. Sakagashira S, Hiddinga HJ, Tateishi K, et al. S20G mutant amylin exhibits increased in vitro amyloidogenicity and increased intracellular cytotoxicity compared to wild-type amylin. Am J Pathol. 2000;157:2101–2109.

21. Cao P, Tu LH, Abedini A, et al. Sensitivity of amyloid formation by human islet amyloid polypeptide to mutations at residue 20. J Mol Biol. 2012;421:282–295.

22. Meier DT, Entrup L, Templin AT, et al. The S20G substitution in hIAPP is more amyloidogenic and cytotoxic than wild-type hIAPP in mouse islets. Diabetologia. 2016;59:2166–2171.

23. Fauchere JL, Charton M, Kier LB, Verloop A, Pliska V. Amino-acid side-chain parameters for correlation studies in biology and pharmacology. Int J Pept Protein Res. 1988;32:269–278.

24. Pace CN, Scholtz JM. A helix propensity scale based on experimental studies of peptides and proteins. Biophys J. 1998;75:422–427.

25. Lyu PC, Sherman JC, Chen A, Kallenbach NR. Alpha-helix stabilization by natural and unnatural amino-acids with alkyl side-chains. Proc Natl Acad Sci U S A. 1991;88:5317–5320.

26. Wiltzius JJW, Sievers SA, Sawaya MR, et al. Atomic structure of the cross-beta spine of islet amyloid polypeptide (amylin). Protein Sci. 2008;17:1467–1474.

27. Luca S, Yau WM, Leapman R, Tycko R. Peptide conformation and supramolecular organization in amylin fibrils: Constraints from solid-state NMR. Biochemistry. 2007;46:13505–13522.

28. Nelson R, Sawaya MR, Balbirnie M, et al. Structure of the cross-beta spine of amyloid-like fibrils. Nature. 2005;435:773–778.

29. Scherzinger E, Sittler A, Schweiger K, et al. Self-assembly of polyglutamine-containing Huntington fragments into amyloid-like fibrils: Implications for Huntington's disease pathology. Proc Natl Acad Sci U S A. 1999;96:4604–4609.

30. Tsai HH, Reches M, Tsai CJ, Gunasekaran K, Gazit E, Nussinov R. Energy landscape of amyloidogenic peptide oligomerization by parallel-tempering molecular dynamics simulation: Significant role of Asn ladder. Proc Natl Acad Sci U S A. 2005;102:8174–8179.

31. Koo BW, Hebda JA, Miranker AD. Amide inequivalence in the fibrillar assembly of islet amyloid polypeptide. Protein Eng Des Sel. 2008;21:147–154.

32. Levine H. Thioflavine-t interaction with synthetic Alzheimers-disease beta-amyloid peptides - detection of amyloid aggregation in solution. Protein Sci. 1993;2:404–410.

33. Buchanan LE, Maj M, Dunkelberger EB, Cheng PN, Nowick JS, Zanni MT. Structural polymorphs suggest competing pathways for the formation of amyloid fibrils that diverge from a common intermediate species. Biochemistry. 2018;57:6470–6478.

34. Goldsbury CS, Cooper GJS, Goldie KN, et al. Polymorphic fibrillar assembly of human amylin. J Struct Biol. 1997;119:17–27.

35. Zhao J, Yu XA, Liang GZ, Zheng J. Structural polymorphism of human islet amyloid polypeptide (hIAPP) oligomers highlights the importance of interfacial residue interactions. Biomacromolecules. 2011;12:210–220.

36. Goldsbury C, Goldie K, Pellaud J, et al. Amyloid fibril formation from full-length and fragments of amylin. J Struct Biol. 2000;130:352–362.

37. Buchanan LE, Dunkelberger EB, Tran HQ, et al. Mechanism of IAPP amyloid fibril formation involves an intermediate with a transient beta-sheet. Proc Natl Acad Sci USA. 2013;110:19285–19290.

38. Dunkelberger EB, Buchanan LE, Marek P, Cao P, Raleigh DP, Zanni MT. Deamidation accelerates amyloid formation and alters amylin fiber structure. J Am Chem Soc. 2012;134:12658–12667.

39. Shim SH, Gupta R, Ling YL, Strasfeld DB, Raleigh DP, Zanni MT. Two-dimensional IR spectroscopy and isotope labeling defines the pathway of amyloid formation with residue-specific resolution. Proc Natl Acad Sci U S A. 2009;106:6614–6619.

40. Abedini A, Raleigh DP. Incorporation of pseudoproline derivatives allows the facile synthesis of human IAPP, a highly amyloidogenic and aggregation-prone polypeptide. Org Lett. 2005;7:693–696.

41. Marek PJ, Patsalo V, Green DF, Raleigh DP. Ionic strength effects on amyloid formation by amylin are a complicated interplay among Debye screening, ion selectivity, and Hofmeister effects. Biochemistry. 2012;51:8478–8490.

42. Case DA, Ben-Shalom IY, Brozell SR, et al. AMBER 2018. San Francisco: University of California, 2018.

43. Nguyen H, Roe DR, Simmerling C. Improved generalized born solvent model parameters for protein simulations. J Chem Theory Comput. 2013;9:2020–2034.

44. Khoury GA, Smadbeck J, Tamamis P, Vandris AC, Kieslich CA, Floudas CA. Forcefield_NCAA: Ab initio charge parameters to aid in the discovery and design of therapeutic proteins and peptides with

unnatural amino acids and their application to complement inhibitors of the compstatin family. ACS Synth Biol. 2014;3:855–869.

SUPPORTING INFORMATION

Additional supporting information may be found online in the Supporting Information section at the end of this article.